Microscopy, 2022, **71(5)**, 262–270
DOI: https://doi.org/10.1093/jmicro/dfac024
Advance Access Publication Date: 10 May 2022
Article

MICROSCOPY

Whole-cell observation of ZIO-stained Golgi apparatus in rat hepatocytes with serial block-face scanning electron microscope, SBF-SEM

Kohei Johkura[1], Nobuteru Usuda[1,2,3,*], Yoshihiro Tanaka[3], Motoaki Fukasawa[4], Kazuyoshi Murata[5], Toru Noda[6,2] and Nobuhiko Ohno[7,8,*]

[1]Department of Histology and Embryology, Shinshu University School of Medicine, 3-1-1 Asahi, Matsumoto, Nagano 390-8621, Japan
[2]Department of Cell Biology and Anatomy, Fujita Health University School of Medicine, 1-98 Dengakugakubo, Kutsukake-cho, Toyoake, Aichi 470-1192, Japan
[3]Graduate School of Engineering, Nagoya Institute of Technology, Gokiso-cho, Showa-ku, Nagoya, Aichi 466-8555, Japan
[4]Department of Biomedical Molecular Sciences (Anatomy II), Fujita Health University School of Medicine, 1-98 Dengakugakubo, Kutsukake-cho, Toyoake, Aichi 470-1192, Japan
[5]National Institute for Physiological Sciences, National Institutes of Natural Sciences, 38 Nishigonaka, Myodaiji, Okazaki, Aichi 444-8585, Japan
[6]Department of Occupational Therapy (Anatomy), Biwako Professional University of Rehabilitation, 967 Kitasakacho, Higashiomi, Shiga 527-0145, Japan
[7]Department of Anatomy, Division of Histology and Cell Biology, Jichi Medical University, 3311-1 Yakushiji, Shimotsuke, Tochigi 329-0498, Japan
[8]Division of Ultrastructural Research, National Institute for Physiological Sciences, 5-1 Myodaiji-Higashiyama, Okazaki, Aichi 444-8787, Japan
[*]To whom correspondence should be addressed. E-mail: usudakenbikyou@gmail.com (N.U.); oonon-tky@umin.ac.jp (N.O.)

Abstract

The Golgi apparatus, which plays a role in various biosynthetic pathways, is usually identified in electron microscopy by the morphological criteria of lamellae. A 3-dimensional analyses with serial block-face scanning electron microscope (SBF-SEM), a volume-SEM proficient in obtaining large volumes of data at the whole-cell level, could be a promising technique for understanding the precise distribution and complex ultrastructure of Golgi apparatus, although optimal methods for such analyses remain unclear since the observation can be hampered with sample charging and low image contrast, and manual segmentation often requires significant manpower. The present study attempted the whole-cell observation and semi-automatic classification and segmentation of the Golgi apparatus in rat hepatocytes for the first time by SBF-SEM via ZIO staining, a classical osmium impregnation. The staining electron-densely visualized individual Golgi lamellae, and their ultrastructure could stably be observed without any noticeable charging. The simple thresholding of the serial images enabled the efficient reconstruction of the labeled Golgi apparatus, which revealed plural Golgi apparatus in one hepatocyte. The combination of the heavy metal-based histochemistry of zinc, iodine and osmium (ZIO) staining and SBF-SEM was useful in the 3-dimensional observation of the Golgi apparatus at the whole-cell level because of two technical advantages: (i) visualization of the Golgi apparatus without any heavy metal staining and efficient acquisition of the block-face images without additional conductive staining or any devices for eliminating charging; (ii) easy identification of the staining and hassle-free, semi-automatic classification and segmentation by simple thresholding of the images. This novel approach could elucidate the topographic characteristics of the Golgi apparatus in hepatocytes.

Key words: SBF-SEM, histochemistry, semi-automatic 3-D reconstruction, Golgi apparatus, whole hepatocyte

Introduction

Serial block-face scanning electron microscope (SBF-SEM) [1,2], a volume-SEM technique [3,4], is potent for imaging and analyzing the 3-dimensional (3-D) ultrastructure of cells and tissues and becoming widely used for this purpose. SBF-SEM is a fully automated volume SEM, which uses a slicing approach with a diamond knife built into the SEM chamber for removing a thin layer of the sample surface. The serially exposed smooth block-face is automatically repeatedly imaged generating aligned serial images [3]. Although nearly full automation in the SBF-SEM observation has been attained, difficulties exist such as the distortion of images in the observation step of resin-embedded tissue specimens due to their charging [5] and boring and the time-consuming reconstruction steps of the digital image volumes obtained [5–8]. In this study, a novel approach of SBF-SEM was assessed via the visualization of the hepatic Golgi apparatus.

The Golgi apparatus is an organelle that functions in different biosynthetic pathways and is involved in the post-translational modification of synthesized proteins by glycosylation [9], sorting/packaging cell products in membrane-bound granules before their use for secretion and vesicle

Received 8 December 2021; Revised 25 April 2022; Editorial Decision 5 May 2022; Accepted 6 June 2022

traffic [10]. In early light and electron microscopic studies, metallic impregnation established their lamellar structure, cisternae, present in nearly all eukaryotic cells. Many cell types contain the Golgi apparatus that is usually localized in a juxta-nuclear site, the apical pole of the nucleus. The Golgi stack of lamellae has morphologically polarized two faces, namely convex-outer *cis* surface and concave-inner *trans* surface. The secretory product moves from *cis* to *trans* surface [11,12]. To better understand the fine structural aspects of the Golgi apparatus at a whole-cell level, the methods for labeling as well as observation of large volumes of the cells or tissues are required.

The identification of the Golgi apparatus composed mainly of stacked cisternae or lamellae as a morphological entity was established by electron microscopy employing metallic impregnation at the beginning of the 1950s [13,14], although osmium impregnation is positive only in *cis*-most lamella [15]. Uneven distribution of the reaction products in cytochemical procedures may result from compositional heterogeneity among different lamellae in the Golgi stacks [10]. The differences among Golgi cisternae have been best documented in the case of hepatocytes, i.e. 5′-nucleotidase, adenylate cyclase and periodic acid-silver methenamine in all lamellae, in contrast, acid phosphatase and thiamine pyrophosphatase only in the *trans* most lamella. Furthermore, ZIO staining, a kind of classical histochemical method using osmium impregnation [16,17], has been employed on the observation of the Golgi apparatus with all lamellae being positive [18]. The Golgi apparatus is a complex organelle variable in the fine structure composed not only of flattened cisternae but also of numerous membranous tubules and vesicles [10]. Due to this complexity of the ultrastructure, because its 3-D structure could not have been visualized on a limited number of ultrathin sections, it was hard to recognize Golgi apparatus as a single organelle. In order to address this concern, high-resolution SEM, high-voltage electron microscope (HVEM) and volume-SEM techniques have been employed [19,20]. By using HVEM stereoscopy, the continuity of cisternal stacks could be demonstrated, thereby establishing the notion of the Golgi apparatus as a single organelle consisting of a branching and anastomosing ribbon, which forms a juxta- or perinuclear network. The 3-D features obtained with HVEM on the organelles selectively stained with heavy metals in thick sections vary among mammalian cell types [21].

A remarkable advance has been made in the SEM technology on the observation of serial surfaces of epoxy resin-embedded tissue specimen together with the computer-based reconstruction of 3-D ultrastructure. The four kinds of volume-SEM techniques, SBF-, focused ion beam (FIB)-, array- and automated tape-collecting ultramicrotome (ATUM)-SEM [3,4,22,23], employing backscattered electron mode [24] during the observation, made it possible to acquire the serial images of materials both at high resolution and in the wide field area of the cells and tissues and became indispensable techniques in the correlative light and electron microscopy (CLEM) [25,26]. Since processing with 3-D imaging software enables mapping and 3-D reconstruction of whole cells from the images obtained by volume SEM, this approach could be promising to analyze distribution and ultrastructure of the Golgi apparatus at the whole-cell level when combined with the labeling of the Golgi apparatus.

The objective of the present study was to enhance the SBF-SEM observation technique by combining it with ZIO staining to overcome the aforementioned difficulties. The technical advantages obtained via this combination have been reported here along with the biological findings on the Golgi apparatus in hepatocytes at the whole-cell level. When the present study was generalized, it is suggested that the combination of heavy metal-based histochemistry and SBF-SEM imaging can elucidate the ultrastructure of cell organelles in cells and tissues.

Methods

Tissue processing for ZIO staining

Ten male Wistar rats (8-week-old) were employed in the study, including the preliminary experiments. They were deeply anesthetized with sodium pentobarbital (80 mg/kg, *i.p.*) and intracardially perfused from the left ventricle with 2.5% glutaraldehyde in 0.1 M sodium phosphate, pH 7.4 for 15 min. All procedures were approved by the Institutional Animal Care and Use Committee of Fujita Health University, Toyoake, Japan. The liver tissues were trimmed into about 1 mm^3 blocks and then immersed in the same fixative for 3 hr. ZIO staining was made following the procedure as previously reported [18,21]. After brief rinsing with Tris-HCl buffer (50 mM Tris-HCl, pH 7.4, 50 mM NaCl, 5 mM $CaCl_2$ and 15 mM $MgCl_2$), the tissue blocks were soaked in the ZIO solution for 100 hr at 4°C. Shortly before the incubation, the ZIO solution was prepared as follows: 3 g Zn powder was suspended in 20 ml distilled water, and 1 g iodine crystal was slowly added to the Zn suspension with stirring. After cooling of the solution to room temperature, the mixture was filtered, and 4 ml of this solution was mixed with 2 ml of the Tris-HCl buffer and 2 ml of 2% osmium tetroxide aqueous solution. After dehydration in graded series of ethanol and acetone, tissues were embedded in an epoxy resin, Epok 812 (Oken Shoji Co., Tokyo, Japan).

Conventional light microscopy and transmission electron microscopy (TEM)

Thin sections of 1 μm were cut on an ultramicrotome and collected on glass slides. The reaction products in the cytoplasm of hepatocytes were string-shaped; however, in other parts, their cytoplasm was black-colored (data not shown). Tissue areas with string-shaped reaction products in the cytoplasm (Fig. 1a) were selected by trimming so that ultrathin sections of 0.1 μm thickness were cut on an ultramicrotome. They were observed through a JEM1010 transmission electron microscope (JEOL Ltd, Tokyo, Japan) at an accelerating voltage of 80 kV without any additional electron staining. The tissue areas with Golgi lamellae positive for the staining, judged by light and transmission electron microscopic observation (Fig. 1b and c) were subjected to SBF-SEM observation.

SBF-SEM observation

SBF-SEM observation was conducted as reported previously [5–8,27]. Small pieces of block (ca. 0.5 × 0.5 × 0.5 mm) were trimmed and mounted on aluminum rivets using Circuit Works Conductive Epoxy (Chemtronics, Kennesaw, GA, USA). The entire surface of the specimen was coated with a thin layer (20 nm thickness) of gold to dissipate the electric

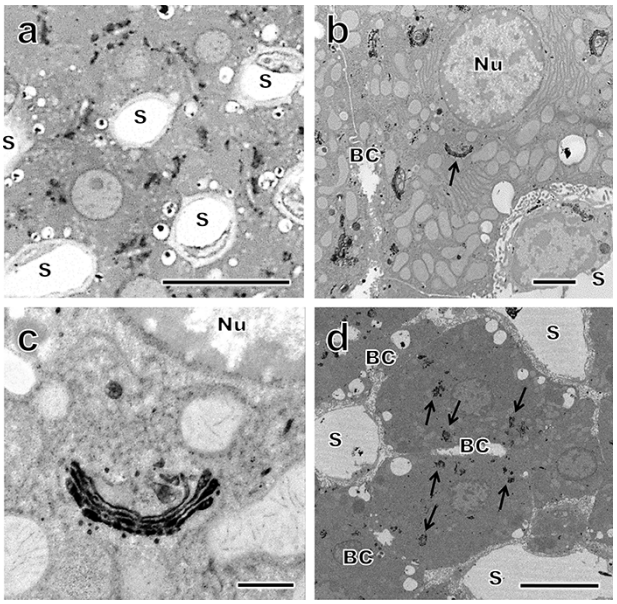

Fig. 1. Representative microscopic images of ZIO-stained hepatocytes. (a) Light micrograph of the rat liver tissue stained by ZIO method. Note the black reaction products located near nuclei and along bile canaliculi in hepatocytes, which are observable without any additional staining. S: sinusoid, Scale bar = 50 μm. (b) Transmission electron micrograph of the rat liver tissue stained by ZIO method without additional electron staining. Note that Golgi lamellae are electron-densely stained (arrow) and other kinds of cellular structures, mitochondria and nuclei are also visualized. Nu: hepatocyte nucleus, BC: bile canaliculus. Scale bar = 2 μm. (c) High-power magnification electron micrograph of the Golgi apparatus indicated by the arrow in b. Note that all lamellae are positive for the staining. Scale bar = 500 nm. (d) A block-face image obtained by SBF-SEM observation shows multiple electron-dense Golgi apparatus (arrows) in ZIO-stained hepatocytes without any additional staining. Scale bar = 5 μm.

charge caused by electron-beam irradiation during SEM imaging. An SBF-SEM system was employed, in which an in-chamber ultramicrotome system (3View; Gatan Inc., Pleasanton, CA, USA) was incorporated in an SEM (MERLIN, Carl Zeiss Microscopy, Jena, Germany). SBF images were acquired at the depth thickness of 70 nm using a backscattered electron detector. The acceleration voltage was 1.1 kV. The pixel size was 10.0 nm/pixel in width and 10.0 nm/pixel in height. The hepatocytes located in the mid-lobular zone of the hepatic lobule [28] were studied.

3-D reconstruction of images obtained by SBF-SEM

The contrast of the images was inversed before data processing. The size of images was reduced from 16 to 8 bit. The image stacks were automatically aligned in a Fiji/ImageJ software package (http://fiji.sc/Fiji). The image stacks were introduced to Amira software (Thermo Fisher Scientific, Tokyo, Japan) and Imaris software, ver. 5.3 (Carl Zeiss Microscopy, Jena, Germany). The classification of the images and segmentation of the stained Golgi apparatus, sinusoids and bile canaliculi were performed semi-automatically by simple thresholding on serial images based on the signal intensity of 256-level grayscale, which could detect Golgi lamellae and exclude the small objects other than Golgi apparatus. Thus, signal intensity was adjusted in order to detect all Golgi lamellae by comparing the lamellae classified and original 8-bit 2D-images. Manual segmentation was made on the contours of the hepatocytes and the nuclei. Twenty cells present in 1560 pictures were analyzed, and 3-D reconstruction was carried out. Quantitative analyses based on surface area data were performed to determine the ratio of the volume in the cytoplasm, the size and the number of labeled Golgi apparatus. Statistical analyses were made by the one-way analysis of variance method. Snapshots and movies of 3-D models used in the figures and Supplementary data were obtained using Amira and Imaris software without further image processing.

Results

Light and transmission electron microscopy and SBF-SEM observation of hepatocytes with ZIO staining

The ZIO-stained hepatocytes located in the mid-lobular zone of the hepatic lobule were observed by light and transmission electron microscopies and SBF-SEM. The SBF-SEM observation noticeably visualized the ultrastructural images that were often vulnerable to sample charging. Black strings or dots showing the Golgi apparatus were located near nuclei and along bile canaliculi by light microscopy (Fig. 1a), which was discriminated by TEM (Fig. 1b). The Golgi apparatus was electron-densely stained and present in the cytoplasm near the nuclei and the bile canaliculi but absent in the cytoplasm close to the sinusoidal capillaries (Fig. 1b). The nucleus and other cell organelles like mitochondria were visible due to the high electron density of the plasma membrane. By high-power magnification picture, Golgi lamellae were densely stained from *cis* to *trans* surface sides (Fig. 1c). In the picture, one Golgi apparatus with 4–5 lamellae are densely stained, in which the *cis*-most one had fenestrations and the *trans* surface accompanied by small vesicles and vacuoles. In the SBF-SEM observation, in addition to the electron-dense Golgi apparatus, the shapes of hepatocytes, nuclei, bile canaliculi and sinusoids were well visualized (Fig. 1d). The Golgi apparatus was stably visualized against various cellular ultrastructures without noticeable charging artifacts, although specimens were processed without any additional heavy metal staining, including the electron staining of uranyl acetate and lead aspartate, and osmium-thiocarbohydrate, which are all employed in the common sample preparation procedure of SBF-SEM observation [5–8,27]. Because the block-face images appeared quite similar to the conventional TEM images and exhibited contrast high enough to identify the Golgi apparatus, bile canaliculi and hepatocytes, the easy identification and hassle-free semi-automatic classification and segmentation of these structures could be performed only by the simple thresholding of the images. These results indicate that the Golgi apparatus along with the fine structure of hepatocytes could well be observed by ZIO staining combined with light and transmission electron microscopes and SBF-SEM.

3-D ultrastructure of the Golgi apparatus in hepatocytes observed by ZIO staining and SBF-SEM

Figure 2 depicts the process of 3-D reconstruction of the Golgi apparatus in a hepatocyte from the SBF images obtained by SBF-SEM (Fig. 2a). Digital micrograph images were con-

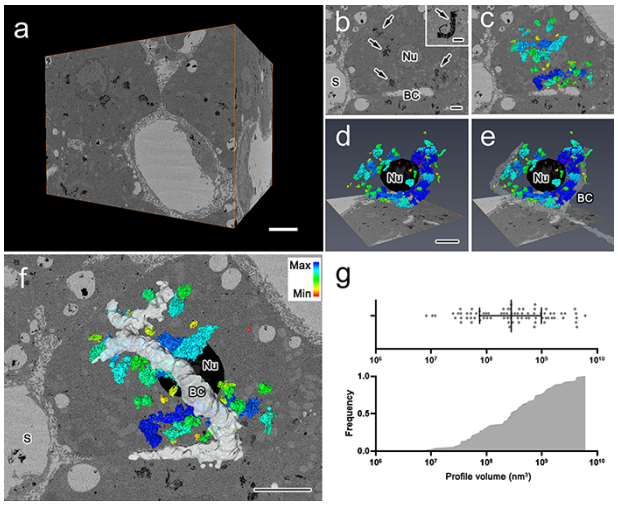

Fig. 2. The process of 3-D reconstruction of individual Golgi apparatus in ZIO-stained hepatocytes on the images obtained by SBF-SEM by Amira software. (a) Reconstruction of serial EM images of the ZIO-stained hepatocytes. Scale bar = 5 μm. (b) One of the serial EM images shows the Golgi apparatus with the lamellar structure of high electron density (arrows) among bile canaliculi (BC), sinusoids (S) and nuclei of hepatocytes (Nu). Scale bar = 2 μm; 500 nm in inset. (c) Each profile of Golgi apparatus was reconstructed and colored according to its size. (d, e) Profiles of nucleus (black) and bile canaliculus (white) were added successively. Scale bar = 5 μm. (f) The reconstruction image centering bile canaliculus shows profiles of the Golgi apparatus, whose colors indicate the volumes of individual profiles ranging from 8.0×10^6 (Min; red) to 6.1×10^9 nm^3 (Max; blue). Note that the Golgi apparatus is aligned along BC and far from sinusoids. Scale bar = 5 μm. A movie corresponding to this figure is presented as Supplementary movie 1. (g) The cumulative frequency distribution (bottom) and the scatter plot (top) of the volume of reconstructed Golgi apparatus in the single hepatocyte in f. Vertical lines in the scatter plot indicate the median and interquartile range.

verted to 8-bit tiff images, and then the Golgi apparatus were recognized depending on the lamellar aspect and the intensity on individual images by visual judgment (Fig. 2b). After 3-D reconstruction by surface rendering, the Golgi apparatus was processed for coloring (Fig. 2c). The nuclei and the bile canaliculi were also colored to visualize the 3-D relationship between different Golgi apparatus (Fig. 2d and e). The resultant image clearly showed that the Golgi apparatus was located near the bile canaliculi, not near the sinusoids (Fig. 2f, Supplementary movie 1). Additionally, isolation and reconstruction of individual profiles of labeled Golgi apparatus facilitated the measurement of their volume, which ranged approximately from 8×10^6 nm^3 to 6×10^9 nm^3 (Fig. 2g). These results demonstrate that the 3-D ultrastructure of hepatocytes was visualized along with the Golgi apparatus, while specimens were processed only with ZIO-staining protocol.

Semi-automatic processing enabled 3-D reconstruction to be hassle-free, as well as the visualization and quantification of the number of hepatocytes. Figure 3 shows the results of the Golgi apparatus in the whole hepatocytes in the midlobular zone of the hepatic lobule. The 3-D structure was reconstructed automatically by surface rendering, thus revealing the location of the Golgi apparatus in the whole hepatocytes. Twenty hepatocytes were reconstructed; of which, eight (four each in single- and bi-nucleated hepatocytes) in Supplementary movies 2–9 were wholly reconstructed with their cytoplasm (Fig. 3a and b, Supplementary movies 2–9). The arrangement of the Golgi apparatus in the cytoplasm was similar among the hepatocytes whose 3-D structure was visualized. At higher magnification, ribbon-like structures were observed and their concave (*cis*) or convex (*trans*) surface was directed randomly, facing not always to bile canaliculi or the nucleus (Fig. 3c and d, Supplementary movies 10, 11). The data processing conducted with the present technique on the plural number of cells enabled the quantitative comparison of the hepatocytes. The quantitative data for the Golgi apparatus and hepatocyte cytoplasm were calculated based on their surface areas, and the average relative volume of the Golgi apparatus to the cytoplasm was obtained to be $1.33 \pm 0.07\%$ in the 20 cells. Separate assessment of single- and bi-nucleated hepatocytes showed rather larger relative volume in bi-nucleated than in single-nucleated hepatocytes, although this difference was not statistically significant (Fig. 4a). On the analysis conditions employed here, each hepatocyte that was wholly reconstructed contained plural Golgi apparatus in average number of 35.4 ± 4.3 (Fig. 4b) and average size of 1.12 ± 0.10 μm^3 (Fig. 4c). Both the number and the size tended to be larger in bi-nucleated than in single-nucleated hepatocytes, although the difference was not statistically significant with $P = 0.05$.

From these results, the whole-cell observation of rat hepatocytes with ZIO staining and SBF-SEM highlighted the morphological characteristics of the Golgi apparatus in hepatocytes. The combination of these techniques enabled the hassle-free, semi-automatic imaging and 3-D reconstruction of a large number of cells due to the techniques' ability to observe a relatively large volume of the tissue and stably acquire high-contrast images of the ultrastructure of the organelles.

Discussion

Technical advantages of the combination of ZIO staining and SBF-SEM observation

In this study, two technical advantages were observed in the combination of the classical ZIO staining and SBF-SEM observation in the 3-D electron microscopic visualization of the Golgi apparatus: (i) efficient acquisition of the block-face images without additional heavy metal staining and conductive staining or any devices for eliminating charging and (ii) easy identification of the staining and hassle-free, semi-automatic classification and segmentation using simple thresholding of the images in the computer-based reconstruction of the 3-D ultrastructure.

The first advantage is that the fine structure of ZIO-stained hepatocytes could be appropriately observed by both conventional light and transmission electron microscopes and SBF-SEM, which makes the acquisition of the images efficient. Various cellular ultrastructures were also 3-dimensionally visualized along with the Golgi apparatus, while specimens were processed only with ZIO-staining protocol. Heavy metals in the ZIO-staining solution [18,21], including zinc, iodine and osmium, may facilitate the imaging of not only the Golgi apparatus but also other ultrastructure in the imaging with conventional electron microscopy and SBF-SEM. Furthermore, the block-face images were stably obtained without conductive staining. In the SBF-SEM observation of resin-embedded tissues, the surface of a resin block is observed by backscattered electron mode along with scanning with an electron beam. Scanning of the electron beam can cause

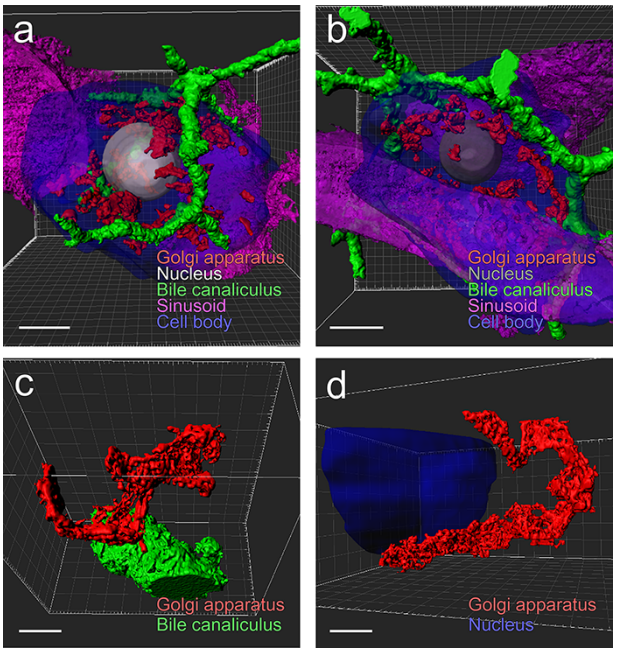

Fig. 3. 3-D reconstruction of single-nucleated and bi-nucleated hepatocytes and their Golgi apparatus obtained on the images obtained by SBF-SEM by Imaris software. (a, b) Snapshots of the 3-D structure of a whole hepatocyte with single nucleus (a) and bi-nucleus (b), which were reconstructed from 200 SBF-SEM micrographs, showing the location of the Golgi apparatus. Note that plural Golgi apparatus are aligned along with the bile canaliculi and near the nucleus; however, they are absent near the sinusoidal capillaries in both types of cell. Golgi apparatus: red, bile canaliculi: green, sinusoid: purple, nucleus: gray, cell body: blue and transparent. Scale bars = 5 μm. Movies of the eight whole hepatocytes are presented as Supplementary movies 2–9 (single-nucleated: 2–5, bi-nucleated: 6–9), in which movies 2 and 6 correspond to Fig. 3a and b, respectively. (c, d) Snapshots of 3-D structure of Golgi apparatus adjacent to the bile canaliculus (c) and the nucleus (d), which were reconstructed from 50 SBF-SEM micrographs. Note that the Golgi apparatus has a twisted ribbon structure. Golgi apparatus: red, bile canaliculus: green, nucleus: blue. Scale bars = 1 μm. Movies of the Golgi apparatus are presented as Supplementary movies 10 and 11, which correspond to Fig. 3c and 3d, respectively.

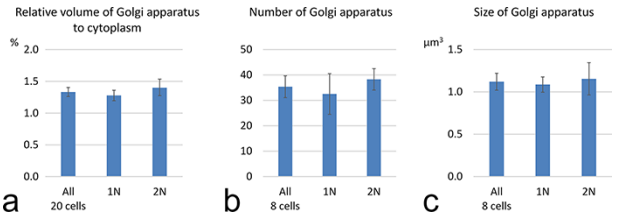

Fig. 4. Quantitative analyses on the Golgi apparatus in 3-D reconstructed single-nucleated and bi-nucleated hepatocytes. (a) The relative volume of the Golgi apparatus to cytoplasm in hepatocytes. The volume was 1.33 ± 0.07% in all 20 cells examined, which in single-nucleated hepatocyte (1 N) was 1.28 ± 0.08% ($n = 11$) and in bi-nucleated hepatocyte (2 N) was 1.40 ± 0.13% ($n = 9$). (b) The number of the Golgi apparatus in one hepatocyte whose cell body was wholly reconstructed. The number was 35.4 ± 4.3 in all eight cells, 32.5 ± 8.0 in 1 N ($n = 4$) and 38.3 ± 4.2 in 2 N ($n = 4$). (c) The size of the Golgi apparatus in one hepatocyte whose cell body was wholly reconstructed. The size was 1.12 ± 0.10 μm^3 in all eight cells, 1.09 ± 0.09 in 1 N ($n = 4$) and 1.15 ± 0.19 in 2 N ($n = 4$). Difference between 1 N and 2 N was not statistically significant in a–c (P- value: 0.05). Values: mean ± SE.

electric charging when the biological specimens are not electron conductive, and the charging distorts signal amplitude and image geometry [23]. This charging is prevented by increasing the conductivity of the specimen using *en bloc* staining with osmium–thiocarbohydrazide–osmium method: OTO and uranyl acetate and lead aspartate to increase the concentration of heavy metals in the specimen [27,29], conductive resins for tissue embedding [5,30] and a device for cyclic in-chamber specimen coating on the sample surface, which is exposed by a diamond knife [23]. Our results suggested that heavy metals in ZIO staining also facilitated SBF-SEM observation without severe charging.

The second advantage is that all the Golgi lamellae from the *cis* to *trans* side can be heavily labeled as shown in the electron micrographs of the present and previous studies [18,21], although some gradient of the density exists from *cis* to *trans*. Compositional heterogeneity of the Golgi lamellae is known to exist based on the results of histochemical staining of hepatocytes [10]. Cytochemical enzyme activities of acid phosphatase and thiamine pyrophosphatase (TPPase) [11] are preferentially detected in *trans* elements of the Golgi apparatus. Contrastively, osmium impregnation can stain *cis*-most cisterna. ZIO staining [15,17] that positively stains all the lamellae (Fig. 1) makes the SBF-SEM observation of the Golgi apparatus easier, especially in the step of classification and segmentation of the image for 3-D reconstruction on PC software, although the substances in the Golgi apparatus labeled with ZIO staining remain poorly understood [17]. In the current study, the 2-D images of ZIO-positive ultrastructures were classified by simple thresholding of the images on the brightness and size due to the high contrast and then subjected to the semi-automatic segmentation and 3-D reconstruction of the Golgi apparatus. Hence, ZIO staining is considered to be a histochemical method suitable for 3-D observation of the Golgi apparatus along with cellular ultrastructure by SBF-SEM and may help artificial intelligence (AI)-based 3-D reconstruction of the Golgi apparatus in whole cells due to the high-contrast labeling of the organelle.

Various TEM and SEM techniques have been attempted for the visualization of the Golgi apparatus at a whole-cell level. Their technical advantages and disadvantages when applied to the 3-D observation of whole cells need to be compared. A direct whole-cell observation of the cells embedded in resin without sectioning were expected to be understood by using HVEM, however, the mammalian cells were too large for the section sickness, which could be observed by HVEM with up to 10 μm at 3000 kV [31]. The 3-D reconstruction of the Golgi apparatus as listed in Table 1 employs serial sectioning TEM (ssTEM) [32,33], in which the sections are manually sectioned and individually observed with TEM, and time-consuming image reconstruction processes are required for 3-D reconstruction. Volume-SEM techniques are intended to be performed with full automation by digitally capturing thousands of serial EM images with minimal human intervention, making it easier, faster and more reliable to acquire tissue volumes for ultrastructural analysis [3]. Volume-SEM techniques can be categorized into two groups: (i) the block-face imaging techniques, FIB-SEM and SBF-SEM and (ii) the array-SEM techniques (alternatively array tomography) [34–36]. ATUM-SEM is one of the array-SEM techniques that uses a section collector automated tape-collecting ultramicrotome [3]. The block-face imaging techniques enable ultrastructural

Table 1. 3-D ultrastructure of the Golgi apparatus in various mammalian cells obtained by whole-cell observation with serial section TEM and volume SEM. The whole-cell observation of the Golgi apparatus in various mammalian cells has been made possible by volume SEM (SBF, FIB and array-SEM) and ssTEM. Each cell in the previous reports has one Golgi apparatus at the perinuclear area except for the megakaryocyte and neural stem cell. The hepatocyte examined in the present study has a high number of Golgi apparatus near the nucleus and bile canaliculi. The cells listed are chronologically arranged

Cell	Number	Location	Method	Author	Journal	Ref.[c]
Parotid acinar cell	One	Perinuclear	ssTEM	Tamaki H	Acta Histochem Cyotochem 1997	32
Pancreatic β cell	One	Perinuclear	ssTEM	Noske AB	J Struct Biol 2007	39
Megakaryocyte[a]	Plural	Perinuclear	FIB-SEM	Eckly A	Blood 2014	34
Epididymal epithelial principal cell	One	Perinuclear	Array-SEM[b]	Koga D	Microscopy (Oxf) 2016	35
Pancreatic acinar cell	One					
Gonadotrope	One					
Neural stem cell	Plural	Perinuclear	SBF-SEM	Taverna E	Sci Rep 2016	40
Purkinje cell	One	Perinuclear	Array-SEM	Koga D	Biomed Res 2017	36
Hepatocyte	Plural	Perinuclear and along bile canaliculi	SBF-SEM	Johkura K	Present paper	

[a]One Golgi apparatus is located beside each lobe of the segmented nuclei in megakaryocytes.
[b]Also termed as array tomography.
[c]Papers are listed in References.

observation by repeatedly removing materials from the surface of a resin block and imaging the block surface via SEM [3]. Thus, they have an advantage of the inherent alignment of serial images. The difference between FIB-SEM and SBF-SEM is the size of the tissue specimen that is deemed suitable for observation and a resin block: a few hundred micrometers with a section thickness of 25–50 nm for SBF-SEM and a few tenths of a micrometer with a section thickness of 3 nm for FIB-SEM [3]. Accordingly, it can be concluded that SBF-SEM is more suitable for the imaging of cell organelles at the whole-cell level, as is performed in the current study. In contrast, FIB-SEM is more suitable for the detailed imaging of cell organelles, especially their internal structures, as shown in a previous study on mitochondrial cristae [37]. In the array-SEM technique, serial ultrathin sections are collected on glass slides or wafers and observed by SEM. CLEM is the distinguished feature of array-SEM and ATUM-SEM, wherein the sections remain after the observation and immunofluorescent staining can be performed on one of the serial sections as described in previous literature [38].

In the present study, the prominent characteristics of the SBF-SEM technique as a volume-SEM technique facilitated the observation of the whole hepatocytes and a greater quantity of cellular images; this was considered to be a suitable EM technique for the reconstruction of the 3-D ultrastructure of the cells.

3-D ultrastructure of the Golgi apparatus obtained with the combination of ZIO staining and SBF-SEM

The combination of ZIO staining and SBF-SEM observation enabled a smooth observation and 3-D reconstruction of the Golgi apparatus in the rat hepatocyte as a whole cell and highlighted the characterization of morphological aspects of the Golgi apparatus in hepatocytes. The new findings on the Golgi apparatus obtained here are, namely, (i) greater number of Golgi apparatus was present in one hepatocyte, (ii) unique localization along the bile canaliculi and near the nucleus, (iii) various directions of the *cis/trans* axis and (iv) the numerical similarity between single- and bi-nucleated hepatocytes.

First, the 3-D reconstruction of hepatocytes visualized plural Golgi apparatus in one hepatocyte. Several studies on the whole-cell reconstruction of vertebrate cells by ssTEM or volume-SEM techniques have revealed the common feature of the Golgi apparatus in mature secretory cells, i.e. the presence of single Golgi apparatus located near the nucleus as summarized in Table 1. ssTEM observation visualized single Golgi apparatus in parotid acinar cells [32] and pancreatic beta cells [39]. Array-SEM visualized single Golgi apparatus in the principal cells of epididymis, pancreatic acinar cells, hypophyseal gonadotropes and cerebellar Purkinje cells [35,36]. In contrast, SBF-SEM revealed plural Golgi apparatus in neural stem cells [40], and FIB-SEM visualized the increase in the number of Golgi apparatus along with the nuclear segmentation of megakaryocytes [34], suggesting that the number of the Golgi apparatus may change during the differentiation of some types of cells. The presence of numerous Golgi apparatus in hepatocytes could be an exceptional feature among mature vertebrate cells.

Second, the unique localization of Golgi apparatus in hepatocytes: the Golgi apparatus were preferentially located near the nucleus, and especially along the bile canaliculi, but absent in the cytoplasm near the sinusoidal capillary. This characteristic localization has long been suggested in the previous light microscopic studies on the osmium impregnated liver tissue [41] and in electron microscopic study [42]. Although morphological and biochemical evidence suggest the presence of a relationship between Golgi apparatus and bile canaliculi, reasons for this unique localization have not yet been fully explained. The hepatocyte cell membrane has plural domains and functional polarity with the bile canaliculi forming the apical membrane domain [43]. Adding to the plasma protein secretion shown by immunoelectron microscopy [44], and the plasma membrane transport [45,46], the formation of bile canaliculi was revealed to involve the Golgi apparatus by administration of fluorescent sphingolipid precursor in differentiated hepatoma cells [47]. The involvement of the Golgi apparatus in the intracellular transport of bile acids before canalicular secretion has been indicated by the

immuno-peroxidase localization of bile salts in the Golgi apparatus [48] and electron microscopic radioautographic localization of radio-labeled bile acid analogs in both the Golgi apparatus and pericanalicular region [49,50]. Biochemical and morphological studies report the important role of the Golgi apparatus in bile secretion also by transporting proteins functioning as bile acids transport, namely ABC transporters BSEP/SPGP and MDR-1 and MDR-2 [51,52]. This series of proteins largely comprises the transport systems at the apical membrane as export pumps for bile salts and other organic solutes [53]. A copper-dependent p-type ATPase, ATP7B, is also transported from the Golgi apparatus to bile canaliculi [54]. Based on these findings, the immediate vicinity between bile canaliculi and the Golgi apparatus may explain the functional relationship between the two.

The third point concerns the *cis/trans* axis of the Golgi apparatus in hepatocytes, regarding lamellae or cisternae. High-voltage electron microscopy has obtained the overall configuration and detailed architecture of the Golgi apparatus of mammalian cells [20]. Farquhar and Palade [10] reported that the constant and most characteristic structural component of the Golgi apparatus (as observed by electron microscope) is a stack of smooth-surfaced cisternae or saccules, which usually have flattened, plate-like centers. The whole structure has a polarity, with the convex side (*cis*) of the stack oriented toward the rough ER and the concave side (*trans*) facing the plasmalemma or the nucleus. The *trans* side of the Golgi apparatus is the secretory side forming secretory vesicles in the cells with single Golgi apparatus (Table 1). Contrastively, hepatic Golgi apparatus in both perinuclear and juxta-bile canalicular sites observed in our SBF-SEM study showed twisted ribbon-like organelles, as described by the HVEM study [33]. Due to this twisted appearance, the hepatic Golgi apparatus does not seem to have a single direction of *cis/trans* axis facing the nucleus, the bile canaliculus or other domains of the cell membrane. Resultantly, the direction of the traffic of putative secretory products is not discernible.

The fourth point is the difference of the Golgi apparatus between single- and bi-nucleated hepatocytes. The relative volume of the Golgi apparatus was about 1% of the cytoplasm based on surface area data. This value was less than that at 6% of the cell volume for the total of Golgi cisternae plus smooth endoplasmic reticulum cisternae, as previously described, although the details of the measurement are not elaborated [55]. The membrane surface area of the Golgi apparatus is estimated at 2% in rat hepatocytes from the data in a monograph [56]. The bi-nucleated hepatocytes have been studied on their characteristics including amitotic nuclear division [57] and have recently drawn attention in relation to liver regeneration [58]. We suggest that the morphological features of the Golgi apparatus in bi-nucleated hepatocytes are not significantly different from those in single-nucleated hepatocytes, although bi-nucleated hepatocytes tend to mark higher value than single-nucleated ones in each parameter.

Conclusion

This is the first study that addressed the electron microscope 3-D reconstruction of biological specimen with the novel combination of heavy metal-based histochemistry, ZIO staining and SBF-SEM applied on the observation of the Golgi apparatus in the serial images of hepatocytes. This combinational technique partially resolved the problems of low image contrast, image deterioration due to sample charging and the time-consuming segmentation step of serial images that hamper the SBF-SEM observation of biological specimens and their subsequent 3-D reconstruction. More concretely, this technique made it possible to visualize the electron-dense images of the Golgi apparatus positive for ZIO staining against various cellular ultrastructures without any additional heavy metal staining to efficiently acquire the block-face images without additional conductive staining or any devices for eliminating charging and to easily identify staining and perform hassle-free semi-automatic classification and segmentation of images for efficient 3-D reconstruction. Consequently, this realized the 3-D observation of a plural number of cells in a large volume of the liver tissue and the characterization of the Golgi apparatus in hepatocytes at a whole-cell level together with the quantitative analysis of their surface areas. When all the steps of the recognition, classification and segmentation of cellular fine structures become possible in the near future via AI-based software, such as deep-learning, this combination of histochemistry and SBF-SEM technology could be applied for analyzing a huge number of cells and visualizing the Golgi apparatus in whole cells in normal and pathological states. It would be helpful in clarifying the pathogenesis of liver diseases by elucidating the 3-D ultrastructure of hepatocytes.

Funding

National Institute for Physiological Sciences and Japan Society for the Promotion of Science KAKENHI (grant number 20K21506); National Center of Neurology and Psychiatry (No. 3–5).

Acknowledgements

The data collection for SBF-SEM was supported by the collaborative research program of National Institute for Physiological Sciences. Authors thank Ms. Atsuko Imai and Mr. Masahiro Ohara (National Institute for Physiological Sciences) and Ms. Itsuki Kinoshita (Fujita Health University) for their helpful technical assistance.

Supplementary data

Supplementary data are available at *Microscopy* online.

Author Contributions

All authors have contributed to this article as follows:

K.J. prepared the manuscript, processed and measured the LM and EM image data;

N.U. planned the whole experiment, developed ZIO-staining procedure for SBF observation and conducted 3-D reconstruction procedures;

Y.T. guided 3-D reconstruction procedures and joined the discussion;

M.F. conducted animal experiments, including tissue processing;

K.M. installed SBF-SEM instruments, guided the observation and established 3-D reconstruction procedures;

T.N. developed ZIO-staining procedure and improved it for SBF observation; and

N.O. conducted SBF-SEM observation, conducted 3-D reconstruction procedures and prepared the manuscript.

References

1. Leighton S B (1981) SEM images of block faces, cut by a miniature microtome within the SEM - a technical note. *Scan. Electron. Microsc.* (Pt 2): 73–76.
2. Denk W and Horstmann H (2004) Serial block-face scanning electron microscopy to reconstruct three-dimensional tissue nanostructure. *PLoS Biol.* 2: e329.
3. Titze B and Genoud C (2016) Volume scanning electron microscopy for imaging biological ultrastructure. *Biol. Cell* 108: 307–323.
4. Kizilyaprak C, Stierhof Y D, and Humbel B M (2019) Volume microscopy in biology: FIB-SEM tomography. *Tissue Cell* 57: 123–128.
5. Nguyen H B, Thai T Q, Saitoh S, Wu B, Saitoh Y, Shimo S, Fujitani H, Otobe H, and Ohno N (2016) Conductive resins improve charging and resolution of acquired images in electron microscopic volume imaging. *Sci. Rep.* 6: 3721.
6. Nakao A, Miyazaki N, Ohira K, Hagihara H, Takagi T, Usuda N, Ishii S, Murata K, and Miyakawa T (2017) Immature morphological properties in subcellular-scale structures in the dentate gyrus of Schnurri-2 knockout mice: a model for schizophrenia and intellectual disability. *Mol. Brain* 10: 60.
7. Ohno N, Chiang H, Mahad D J, Kidd G J, Liu L, Ransohoff R M, Sheng Z H, Komuro H, and Trapp B D (2014) Mitochondrial immobilization mediated by syntaphilin facilitates survival of demyelinated axons. *Proc. Natl. Acad. Sci. USA.* 111: 9953–9958.
8. Miyazaki N, Esaki M, Ogura T, and Murata K (2014) Serial block-face scanning electron microscopy for three-dimensional analysis of morphological changes in mitochondria regulated by Cdc48p/p97 ATPase. *J. Struct. Biol.* 187: 187–193.
9. Roth J and Berger E G (1982) Immunocytochemical localization of galactosyltransferase in HeLa cells: codistribution with thiamine pyrophosphatase in trans-Golgi cisternae. *J. Cell Biol.* 93: 223–229.
10. Farquhar M G and Palade G E (1981) The Golgi apparatus (complex)-(1954–1981)-from artifact to center stage. *J. Cell Biol.* 91: 77s–103s.
11. Novikoff A B and Holtzman E (1976) Chapter 2.5, The Golgi apparatus. In: *Cells and Organelles*, *Second edition*, pp 99–110 (Holt, Rinehart and Winston, New York).
12. Fawcett D W (1966) *An Atlas of Fine Structure, the Cell, Its Organelles and Inclusions*, pp 112–132 (Saunders, Philadelphia).
13. Dalton A J and Felix M D (1956) A comparative study of the Golgi complex. *J. Biophys. Biochem. Cytol.* 2: 79–84.
14. Berger E G (1997) The Golgi apparatus: from discovery to contemporary studies. In: Berger E G and Roth J (eds), *The Golgi Apparatus*, pp 1–35 (Birkhäuser, Basel).
15. Friend D S and Murray M J (1965) Osmium impregnation of the Golgi apparatus. *Am. J. Anat.* 117: 135–149.
16. Champy C H (1913) Granules et substances réduisant l'iodure d'osmium. *J. Anat. Physiol. Norm. Pathol.* 4: 323–343.
17. Hayat M A (1993) Chapter 8, staining and related reagents. In: *Stains and Cytochemical Methods*, pp 173–184 (Plenum Press, New York).
18. Atsuzawa K, Usuda N, Nakazawa A, Fukasawa M, Danev R, Sugitani S, and Nagayama K (2009) High-contrast imaging of plastic-embedded tissues by phase contrast electron microscopy. *J. Electron Microsc. (Tokyo)* 58: 35–45.
19. Tanaka K, Mitsushima A, Fukudome H, and Kashima Y (1986) Three-dimensional architecture of the Golgi complex observed by high resolution scanning electron microscopy. *J. Submicrosc. Cytol.* 18: 1–9.
20. Rambourg A and Clermont Y (1990) Three-dimensional electron microscopy: structure of the Golgi apparatus. *Eur. J. Cell Biol.* 51: 189–200.
21. Noda T and Ogawa K (1984) Golgi apparatus is one continuous organelle in pancreatic exocrine cell of mouse. *Acta Histochem. Cytochem.* 17: 435–451.
22. Ferguson S, Steyer A M, Mayhew T M, Schwab Y, and Lucocq J M (2017) Quantifying Golgi structure using EM: combining volume-SEM and stereology for higher throughput. *Histochem. Cell Biol.* 147: 653–669.
23. Titze B and Denk W (2013) Automated in-chamber specimen coating for serial block-face electron microscopy. *J. Microsc.* 250: 101–110.
24. Hayat M A (1978) *Introduction to Biological Scanning Electron Microscopy. Part 1, Instrumentation*, pp 18–20 (University Park Press, Baltimore).
25. Ohta K, Hirashima S, Miyazono Y, Togo A, and Nakamura K I (2021) Correlation of organelle dynamics between light microscopic live imaging and electron microscopic 3D architecture using FIB-SEM. *Microscopy (Oxf.)* 70: 161–170.
26. Thomas C I, Ryan M A, Scholl B, Guerrero-Given D, Fitzpatrick D, and Kamasawa N (2021) Targeting functionally characterized synaptic architecture using inherent fiducials and 3D correlative microscopy. *Microsc. Microanal.* 27: 156–169.
27. Deerinck T J, Bushong E A, Lev-Ram V, Shu X, Tien R Y, and Ellisman M H (2010) Enhancing serial blockface scanning electron microscopy to enable high resolution 3-D nanohistology of cells and tissues. *Microsc. Microanal.* 16: 1138–1139.
28. Cunningham R P and Porat-Shliom N (2021) Liver zonation - revisiting old questions with new technologies. *Front. Physiol.* 12: 732929.
29. Seligman A M, Wasserkrug H L, and Hanker J S (1966) A new staining method (OTO) for enhancing contrast of lipid-containing membranes and droplets in osmium tetroxide-fixed tissue with osmiophilic thiocarbohydrazide (TCH). *J. Cell Biol.* 30: 424–432.
30. Wanner A A, Genoud C, Masudi T, Siksou L, and Friedrich R W (2016) Dense EM-based reconstruction of the interglomerular projectome in the zebrafish olfactory bulb. *Nat. Neurosci.* 19: 816–825.
31. Martone M E, Deerinck T J, Young S J, and Ellisman M H (1999) Three dimensional protein localization using high voltage electron microscopy. *Acta Histochem. Cytochem.* 32: 35–43.
32. Tamaki H and Yamashina S (1997) Three-dimensional dynamics of the Golgi apparatus in mitotic parotid acinar cells: computer-aided reconstruction from cytochemically-marked ultrathin serial sections. *Acta Histochem. Cytochem.* 30: 643–651.
33. Mogelsvang S, Marsh B J, Ladinsky M S, and Howell K E (2004) Predicting function from structure: 3D structure studies of the mammalian Golgi complex. *Traffic* 5: 338–345.
34. Eckly A, Heijnen H, Pertuy F, Geerts W, Proamer F, Rinckel J Y, Léon C, Lanza F, and Gachet C (2014) Biogenesis of the demarcation membrane system (DMS) in megakaryocytes. *Blood* 123: 921–930.
35. Koga D, Kusumi S, and Ushiki T (2016) Three-dimensional shape of the Golgi apparatus in different cell types: serial section scanning electron microscopy of the osmium-impregnated Golgi apparatus. *Microscopy (Oxf.)* 65: 145–157.
36. Koga D, Kusumi S, Ushiki T, and Watanabe T (2017) Integrative method for three-dimensional imaging of the entire Golgi apparatus by combining thiamine pyrophosphatase cytochemistry and array tomography using backscattered electron-mode scanning electron microscopy. *Biomed. Res.* 38: 285–296.
37. Ohta K, Sadayama S, Togo A, Higashi R, Tanoue R, and Nakamura K (2012) Beam deceleration for block-face scanning electron microscopy of embedded biological tissue. *Micron* 43: 612–620.
38. Koga D, Ushiki T, and Watanabe T (2017) Novel scanning electron microscopy methods for analyzing the 3D structure of the Golgi apparatus. *Anat. Sci. Int.* 92: 37–49.

39. Noske A B, Costin A J, Morgan G P, and Marsh B J (2008) Expedited approaches to whole cell electron tomography and organelle mark-up in situ in high-pressure frozen pancreatic islets. *J. Struct. Biol.* 161: 298–313.
40. Taverna E, Mora-Bermúdez F, Strzyz P J, Florio M, Icha J, Haffner C, Norden C, Wilsch-Bräuninger M, and Huttner W B (2016) Non-canonical features of the Golgi apparatus in bipolar epithelial neural stem cells. *Sci. Rep.* 6: 21206.
41. Cramer W and Ludford R J (1926) On the cellular mechanism of bile secretion and its relation to the Golgi apparatus of the liver cell. *J. Physiol.* 62: 74–80.
42. Fawcett D W (1955) Observations on the cytology and electron microscopy of hepatic cells. *J. Natl. Cancer Inst.* 15: 1475–1503.
43. Gissen P and Arias I M (2015) Structural and functional hepatocyte polarity and liver disease. *J. Hepatol.* 63: 1023–1037.
44. Yokota S (1989) Effect of colchicine on the intracellular transport of secretory proteins in rat liver parenchymal cells. Immunocytochemical observations. *Cell Struct. Funct.* 14: 545–559.
45. Saucan L and Palade G E (1994) Membrane and secretory proteins are transported from the Golgi complex to the sinusoidal plasmalemma of hepatocytes by distinct vesicular carriers. *J. Cell Biol.* 125: 733–741.
46. Sztul E S, Howell K E, and Palade G E (1983) Intracellular and transcellular transport of secretory component and albumin in rat hepatocytes. *J. Cell Biol.* 97: 1582–1591.
47. Zaal K J, Kok J W, Sormunen R, Eskelinen S, and Hoekstra D (1994) Intracellular sites involved in the biogenesis of bile canaliculi in hepatic cells. *Eur. J. Cell Biol.* 63: 10–19.
48. Lamri Y, Roda A, Dumont M, Feldmann G, and Erlinger S (1988) Immunoperoxidase localization of bile salts in rat liver cells. Evidence for a role of the Golgi apparatus in bile salt transport. *J. Clin. Invest.* 82: 1173–1182.
49. Suchy F J, Balistreri W F, Hung J, Miller P, and Garfield S A (1983) Intracellular bile acid transport in rat liver as visualized by electron microscope autoradiography using a bile acid analogue. *Am. J. Physiol.* 245: G681–G689.
50. Goldsmith M A, Huling S, and Jones A L (1983) Hepatic handling of bile salts and protein in the rat during intrahepatic cholestasis. *Gastroenterology* 84: 978–986.
51. Kubitz R, Sütfels G, Kühlkamp T, Kölling R, and Häussinger D (2004) Trafficking of the bile salt export pump from the Golgi to the canalicular membrane is regulated by the p38 MAP kinase. *Gastroenterology* 126: 541–553.
52. Kipp H and Arias I M (2000) Newly synthesized canalicular ABC transporters are directly targeted from the Golgi to the hepatocyte apical domain in rat liver. *J. Biol. Chem.* 275: 15917–15925.
53. Boyer J L (2013) Bile formation and secretion. *Compr. Physiol.* 3: 1035–1078.
54. Ala A, Walker A P, Ashkan K, Dooley J S, and Schilsky M L (2007) Wilson's disease. *Lancet* 369: 397–408.
55. Alberts B, Bray D, Lewis J, Raff M, Roberts K, and Watson J D (1983) Chapter 7, internal membrane and the synthesis of macromolecules. In: *Molecular Biology of the Cell. Part II*, p 321 (Garland Publishing Inc, New York).
56. Blouin A (1983) Anatomy, ultrastructure and morphometry of the liver. In: Glaumann H, Peters Jr. T, and Redman C (eds), *Plasma Protein Secretion by the Liver*, pp 31–53 (Academic Press Inc, London).
57. Omochi S, Nagata N, and Momoze S (1957) Hourly variation of the frequency of cell divisions and the fate of binucleate cells in rat liver (Japanese with English abstract). *Acta Anatomica Nipponica* 32: 416–422.
58. Miyaoka Y, Ebato K, Kato H, Arakawa S, Shimizu S, and Miyajima A (2012) Hypertrophy and unconventional cell division of hepatocytes underlie liver regeneration. *Curr. Biol.* 22: 1166–1175.